Journal of Power Sources 196 (2011) 2179–2186

Contents lists available at ScienceDirect

Journal of Power Sources

journal homepage: www.elsevier.com/locate/jpowsour

Cyclic stability and C-rate performance of amorphous silicon and carbon based anodes for electrochemical storage of lithium

Dongjoon Ahn [1], Rishi Raj [*,1]

Department of Mechanical Engineering, University of Colorado at Boulder, Boulder, CO 80309-0427, United States

ARTICLE INFO

Article history:
Received 23 July 2010
Received in revised form
29 September 2010
Accepted 29 September 2010
Available online 7 October 2010

Keywords:
Lithium anodes
Polymer-derived ceramics
Silicon oxycarbide

ABSTRACT

Polymer-derived, amorphous ceramics (PDCs) constituted from silicon, carbon, oxygen and nitrogen are promising candidates as anodes for lithium ion (Li^+) batteries, having a reversible capacity of up to 800 mAh g^{-1}. These measurements of lithium capacity are extended here to cyclic stability, high C-rate performance, and composition-range. The following new results are presented: (a) materials processed at 800 °C perform better than those synthesized at lower and higher temperatures, (b) materials with high oxygen content perform better than those with high nitrogen, (c) the SiCO materials are highly stable in cyclic loading, and (d) they are robust materials, capable of very high C-rates, without damage to their overall performance. Phenomenological analysis of composition dependent capacity suggests that Li is sequestered to mixed-bond tetrahedra of Si coordinated to both oxygen and carbon; it is argued that when oxygen is substituted by nitrogen the ability of these mixed bonds to bind to lithium in a reversible manner is severely diminished.

1. Introduction

The high capacity of silicon [1] has stimulated renewed interest in alternative materials to carbon [2] for anodes in Li^+ batteries. Silicon carries a theoretical capacity of 4200 mAh g^{-1}, much higher than that of carbon, with 372 mAh g^{-1}. Crystalline silicon, however, suffers from a large volume expansion upon the insertion of lithium [3], which can cause the capacity to fade with charge–discharge cycles [4]. Nevertheless, the discovery has unleashed a plethora of research and development activity that ranges from nanoscale silicon to silicon alloys and composites for anode applications.

Polymer-derived ceramics (PDCs), made from polysiloxanes [5] and polysilazanes [6] represent a new class of materials for reversible storage of Li. They are interesting because they combine Si and C chemistries with O and N. The siloxane based PDCs yield silicon oxycarbide (SiCO), while the silazanes produce oxynitride ceramics (SiCN). Both ceramics are expected to have a molecular structure that is shown in Fig. 1. It consists of a network of graphene, that forms nanodomains, 1–5 nm in size [7]. The silicon tetrahedra have two essential configurations. In one of them, called mixed bonds, the silicon atoms are coordinated to carbon as well as O (and, or N), while the other Si species are carbon free. The mixed bond tetrahedra are anchored to the domain walls, while the carbon free tetrahedra are enclosed within the intradomain regions.

The Li insertion properties for both SiCO and SiCN materials have been reported [5,6]. Generally SiCO can bear much higher capacities than SiCN: about 800 mAh g^{-1} versus <100 mAh g^{-1}. Both materials exhibit considerable first cycle irreversibility, amounting to 25%–35% to the total capacity. In subsequent cycles they show hysteresis, with a higher voltage being required for lithium extraction than for lithium insertion [8]. Despite these negatives, the PDCs are promising for future anode technologies, because of their unusual molecular network structure. The network is more open than would be for crystalline materials of a similar composition (the PDCs have an overall density that is two-thirds that of corresponding crystalline structures). There is no evidence of any phase transformations in these materials below their thermal degradation temperature, which is very high (~1500 °C) [9]. The bonding is strong and stable. The amorphous nature, the high chemical and structural stability, and the low density, are harbingers of fast diffusion, and low volume expansion with Li insertion. The polymer routes to synthesis hold the prospect of changing the chemical nature of the molecular network in order to overcome the irreversible capacity and hysteresis that are presently seen in the PDCs.

Briefly, the PDCs are processed from liquid organic precursors. These liquids are first cross-linked in the 350 °C–400 °C range, when they convert into a hard epoxy. The epoxy is pulverized into a powder, with a particle size in the 10 μm–50 μm range. The powder is then heated in an inert atmosphere to drive out the hydrogen, leaving behind the network shown in Fig. 1. Hydrogen evolution begins at ~700 °C and is completed by ~1000 °C [10]. The likely mecha-

* Corresponding author. Tel.: +1 303 492 1029; fax: +1 303 492 3498.
E-mail address: rishi.raj@colorado.edu (R. Raj).
[1] The authors are or have been affiliated with PDC-Energy, LLC, Louisville, CO, United States.

0378-7753/$ – see front matter © 2010 Elsevier B.V. All rights reserved.
doi:10.1016/j.jpowsour.2010.09.086

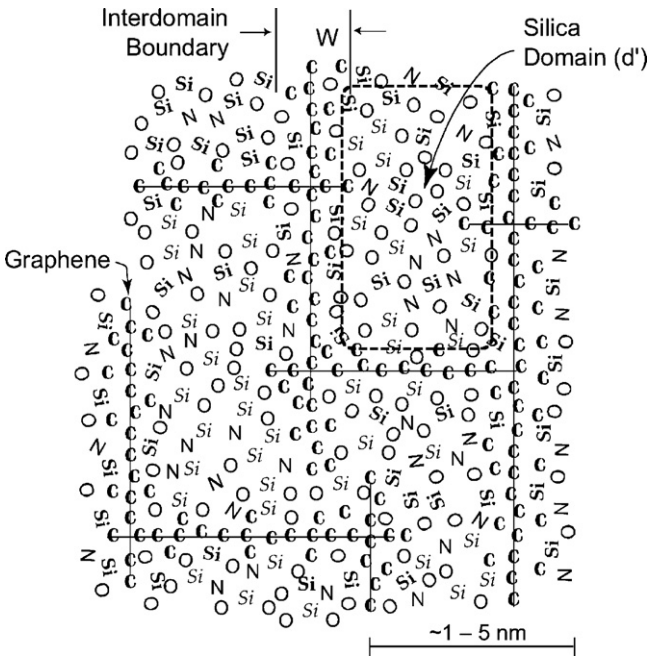

Fig. 1. The nanodomain molecular network structure of SiCNO polymer-derived ceramics.

nism for the formation of graphene networks is that the C–H bonds are broken during pyrolysis, and the carbon atoms, with their dangling bonds, self assemble into the graphene networks. The mobility of carbons is limited since they are bonded to ring structures of Si and O; this inability to move over long distances, is believed to prevent C from precipitating into particles of graphite. It is of note, as shown below, that the samples processed at 800 °C, which are likely to retain some hydrogen, show better cyclic stability than the sample processed at 1000 °C.

The present article presents new results related to the cyclic stability and high C-rate performance of the PDCs. We show that the cyclic stability is related to the processing temperature. The influence of composition is studied since SiCO and SiCN compositions are continuously miscible, yielding samples with variable N/O ratio. While the capacities at the extremes of this range are known, it is of fundamental interest to know how the capacity changes as the N/O ratio is varied. These results, which are included in Appendix A, show a sharp transition from high capacity to low capacity that lies near N/O≈1, raising interesting questions about the energetics of molecular interactions between Li, and Si–C–N–O. The main section of the paper is devoted to the performance of SiCO materials.

2. Materials preparation

Polymer-derived SiCO powders were synthesized by controlled pyrolysis of crosslinked organic polymers. 1,3,5,7-Tetramethyl-1,3,5,7-tetravinylcyclotertrasiloxane (TTCS, Gelest, USA) was used as the organic polymer precursor. 1 wt.% dicumyl peroxide of the amount of TTCS was added to promote crosslinking. The mixed liquid precursor was cross-linked at 380 °C for 5 h in Ar purged furnace (Thermolyne, USA). The crosslinked polymer monolith was ball-milled for 1 h in plastic jar with zirconia balls as the grinding media. The milled powder was pyrolyzed under different conditions (700 °C, 800 °C, 1000 °C, 1200 °C, and 1400 °C) for 5 h under argon purged tubular furnace. Heating rates of cross-link and pyrolysis were 90 °C h^{-1} and 240 °C h^{-1}, respectively. The cooling rates were the same as the heating rates. After full pyrolysis, a black ceramic powder was obtained. Specimens heat-treated at the five temperatures are given the nomenclature, SiCO-7, SiCO-8, SiCO-10, SiCO-12, and SiCO-14.

Powders with varying N/O ratio were synthesized by controlled pyrolysis of crosslinked organic polymers. 1,3,5,7-tetramethyl-1,3,5,7-tetravinylcyclotertrasiloxane (TTCS, Gelest, USA) and Polyureasilazane (CERASET^{TM}, Kion Specialty Polymer, Clariant, USA). After TTCS and Ceraset^{TM} were mixed in various proportions, 1 wt.% dicumyl peroxide of the total amount of TTCS and CERASET solution was added to promote crosslinking. The mixed, liquid precursor was cross-linked at 380 °C for 5 h in Ar purged furnace (Thermolyne, USA). The crosslinked polymer monolith was ball-milled for 1 h in plastic jar with zirconia balls as the grinding media. The milled powder was pyrolyzed at 1000 °C for 5 h under argon purged tubular furnace. Heating rates of cross-link and pyrolysis were 90 °C h^{-1} and 240 °C h^{-1}, respectively. The cooling rates were the same as the heating rates. After full pyrolysis, a black ceramic powder was obtained. Five specimen compositions, called PDC-1 thru PDC-5 were prepared. The compositions of these specimens are given in Appendix A.

Elemental analysis of the SiCO and the SiCNO specimens was done for nitrogen, oxygen, and carbon content. Silicon content was calculated as the difference between the sum of the measured oxygen, nitrogen, and carbon content and the total weight of the specimen. The carbon content was measured by combustion (LECO Corp., Model C-200, USA) method with accelerants as iron chip and Lecocel II HP. The nitrogen and oxygen content were analyzed by fusion (LECO Corp., TC-600, USA) method. Cast iron with 3.36% carbon was used as standard in carbon analysis and tungsten oxide and aluminum nitride were selected as the standards for oxygen and nitrogen analysis.

3. Electrochemical testing

The PDCs electrodes for the measurement of electrochemical properties were prepared by mixing a slurry consisting of 80 wt.% of active material (PDCs), 10 wt.% acetylene black, and 10 wt.% of polyvinylidene fluoride (PVDF) dissolved in 1-methyl-2-pyrrolidinone. The slurry mixture was screen printed on to a copper foil using a doctor blade and a film applicator. This electrode served as the working electrode in a CR 2032-type coin cell. A lithium foil was used as the counter and reference electrode, for a half-cell configuration. Polypropylene-polyethylene-polypropylene tri-layered microporous membrane (Celgard, USA) and 1 M of $LiPF_6$ dissolved in a mixed solvent which was composed of the equal volumetric amount from both Ethylene Carbonate (EC) and Dimethyl Carbonate (DMC) (Novolyte, USA) were used as the separator and the electrolyte, respectively. The coin-cells were assembled, crimped and closed in an argon filled glove box. Nominal, first cycle electrochemical measurements were performed at Li insertion and extraction current density of 100 mA g^{-1}, between voltage limits of 0.01 V and ~3 V. Unsymmetrical cycles were employed for the high C-rate experiments: Li was inserted at the slow rate at a current density of 100 mAh g^{-1}, and then extracted at increasing current densities.

The C-rate can be measured in two ways. In crystalline materials the theoretical upper bound for the capacity is defined by the stoichiometry of the intercalated crystal. For example, in graphite the compound LiC_6 is formed which gives a theoretical capacity of 371 mAh g^{-1}. (The stoichiometric composition of intercalated MesoCarbon MicroBead (MCMB) carbon is $Li_{0.56}C_6$, which translates into a theoretical capacity of 200 mAh g^{-1}.) In these instances the C-rate is written as *nC*, where:

$$n = \frac{i_j}{q_A^o} \quad (1)$$

where i_j the current density in mA g^{-1}, and q_A^o is the upper bound of the theoretical capacity mentioned above, in units of mAh g^{-1}.

A different measure of the C-rate is needed, however, for the amorphous materials of interest in this work, since in an amorphous structure there is a spectrum of energy levels where Li may reside. Thus, it is not possible to define a theoretical value for the capacity: instead it depends on the extent of the loading of Li, and on the current density, $q_A(i_j)$. In this instance it is appropriate to define the C-rate in such a manner that it gives the time required to insert or extract the charge $q_A(i_j)$ at a given value of i_j. This way of measuring the C-rate is given the nomenclature $m\bar{C}$, where

$$m = \frac{i_j}{q_A} \tag{2}$$

Combining Eqs. (1) and (2) gives the relationship between the two C-rates:

$$n = m\frac{q_A}{q_A^o} \tag{3}$$

Throughout this paper the $m\bar{C}$ notation is used to describe the results.

4. Results the influence of N/O ratio in SiCNO specimens

The results for specimens PDC-1 to PDC-5 are given in Appendix A. They can be summarized as follows.

(i) The influence of N/O on the capacity may be separated into two regimes. In the oxygen rich regime the capacity is very high, while it is very low in the nitrogen rich compositions. The transition occurs quickly near N/O≈1.
(ii) The overall composition of the SiCNO samples can be separated into mixtures of stoichiometric SiC, SiO_2 and Si_3N_4, which will form silicon-centered tetrahedra of various coordinations, and "free" carbon according to the following equation:

$$SiC_xO_yN_z = (1 - \frac{y}{2} - \frac{3z}{4})SiC + \frac{y}{2}SiO_2 + \frac{z}{4}Si_3N_4 + (x - 1 + \frac{y}{2} + \frac{3z}{4})C \tag{4}$$

The weight fraction of C in the alloy is then given by:

$$\text{wt.\% C} = \frac{(x - 1 + (y/2) + (3z/4)) \times 12}{28 + x \times 12 + y \times 16 + z \times 14} \times 100 \tag{5}$$

where the whole numbers in Eq. (5) correspond to the atomic weights of Si, C, O, and N. A plot of the capacity of the SiCNO samples, in mAh g^{-1} versus wt.% of C is given in Fig. 2. If the capacity is merely arising from "free" C then the data would fit the theoretical line, as shown. We note that while the nitrogen rich containing samples lie near this theoretical line, the oxygen rich samples lie far above. A detailed analysis of SiCO samples had shown that in these samples the majority of the capacity is related to the mixed bonds which would be contained in the first two terms on the right hand side of Eq. (4); in this same analysis it was shown that the portion of the capacity associated with free carbon agreed well with the theoretical capacity of graphite [11]. In contrast, in the case of nitrogen rich samples, as shown by the plot in Fig. 2, most of the capacity is related to the "free" carbon. This comparison shows that in the presence of nitrogen the mixed bonds formed between Si–C–O become unable to sequester Li.

5. Results: the SiCO specimens

The composition of the SiCO specimens was the same as that of PDC-5 given in Table A1. This composition is shown in the diagram

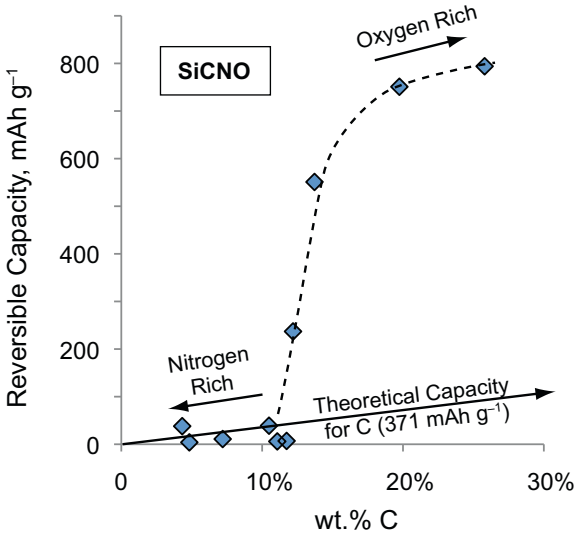

Fig. 2. The partitioning of the capacity into "free" carbon fraction, plotted along the *x*-axis and mixed bonds. The nitrogen rich samples appear to possess only free carbon capacity.

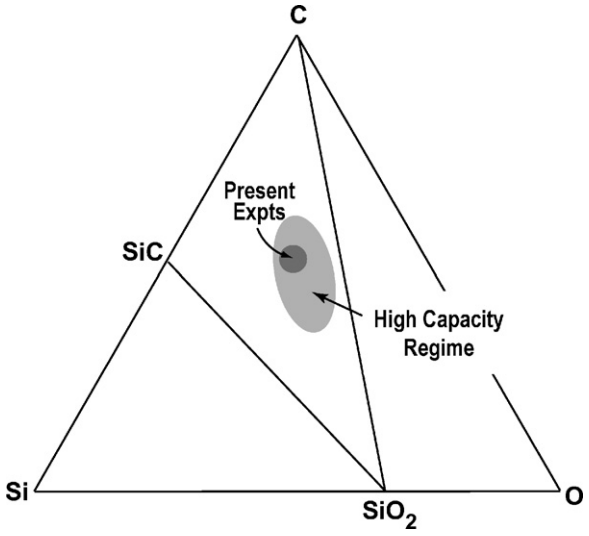

Fig. 3. The composition of the SiCO specimens in the current study.

in Fig. 3: it lies well within the high capacity regime of the SiCO system [11].

The samples were processed at five temperatures, 700 °C, 800 °C, 1000 °C, 1200 °C and 1400 °C, and are designated as SiCO-7, SiCO-8, SiCO-10, SiCO-12, and SiCO-14. The first three cycles data for these specimens is given in Fig. 4. The first cycle total capacity, the reversible capacity, and the first cycle irreversibility, expressed as First (Initial) Cycle Loss (ICL), are listed in Table 1.

Table 1
The first cycle capacity, the reversible capacity, and the first-cycle loss (ILC) expressed as a fraction of the first cycle, for the five samples prepared at different temperatures.

Sample	1st cycle (mAh g^{-1})	Reversible capacity (mAh g^{-1})	ICL (%)
SiCO-7	1076	444	59
SiCO-8	1354	906	33
SiCO-10	1252	958	23
SiCO-12	1124	819	27
SiCO-14	366	88	76

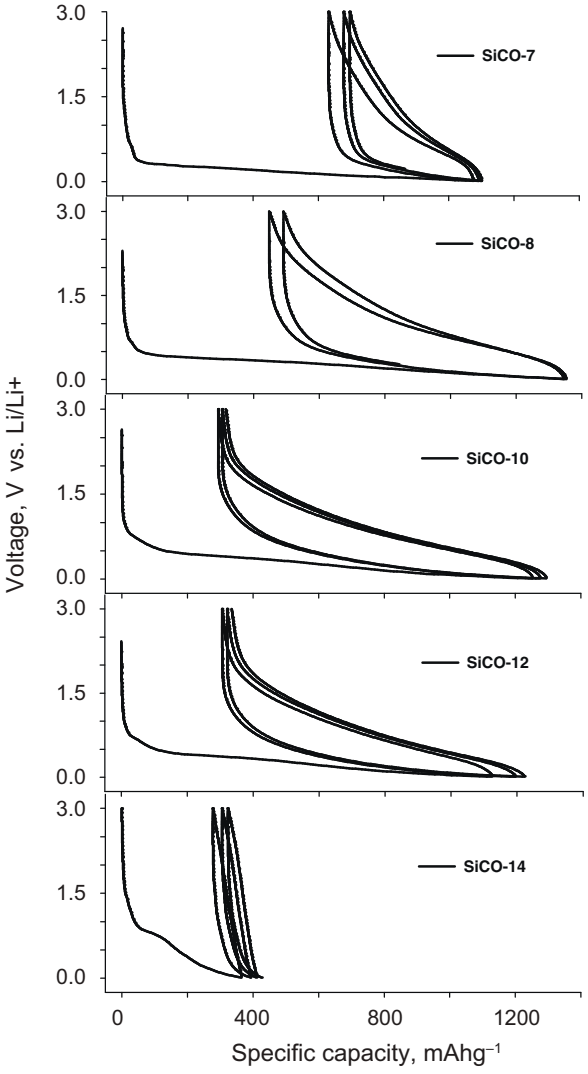

Fig. 4. The first three cycles for the five SiCO specimens processed at different temperatures (the numbers imply the temperature in hundreds, e.g., 7 is 700 °C).

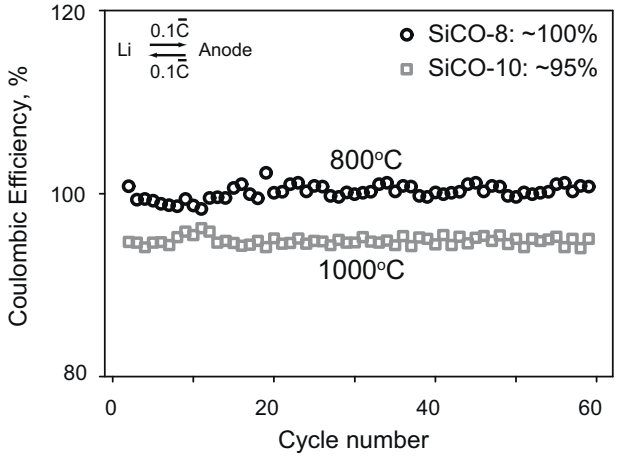

Fig. 6. Coulombic efficiency of specimens processed at 1000 °C and 800 °C.

Taken by themselves, the results in Table 1 would suggest that the best capacity and the lowest ICL is obtained for the samples heat-treated at 1000 °C. It gives a reversible capacity of 958 mAh g^{-1} and an ICL of 23%. The capacity loses ground at lower and higher heat-treatment temperatures. The fall off is especially severe at 700 °C and 1400 °C.

However, further evaluation, in terms of the stability of many cycles, shows that the 800 °C specimen (SiCO-8) performs better than the 1000 °C (SiCO-10) treated sample. These results are given in Fig. 5(a) and (b). While the SiCO-10 sample has a higher capacity early on, it loses capacity with progressive cycling. This behavior is further reflected in the coulombic efficiency, shown in Fig. 6, which remains near 100% for SiCO-8 but falls to 95% for the SiCO-10 specimen.

The capacity was measured as a function of the C-rate, $m\bar{C}$, by operating the cell at progressively increasing the current density. The best performance is obtained for SiCO-8. A comparison with SiCO-10 and with cells prepared with MCMB carbon (Osaka Gas, Japan) (in the same way as the cells with SiCO) is given in Fig. 7(a); the data are plotted using Eq. (2), which employs the measured capacity (as opposed to the theoretical capacity as required by Eq. (1)) of the anode to calculate the C-rate. In these cycles the Li was inserted into the anodes at the rate of 100 mA g^{-1}, which corresponds to ~0.1$\bar{C}$, while the rate

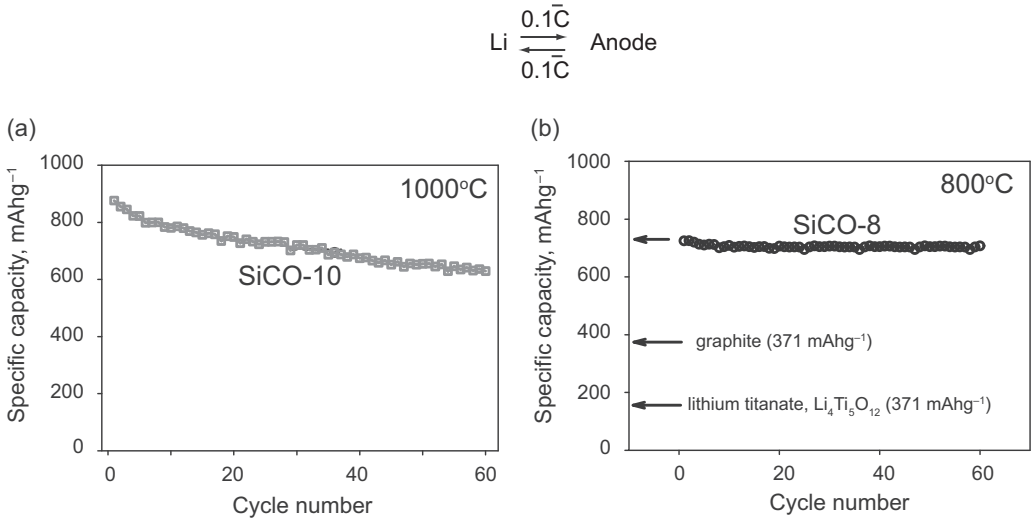

Fig. 5. Cyclic stability of specimens processed at 1000 °C and 800 °C.

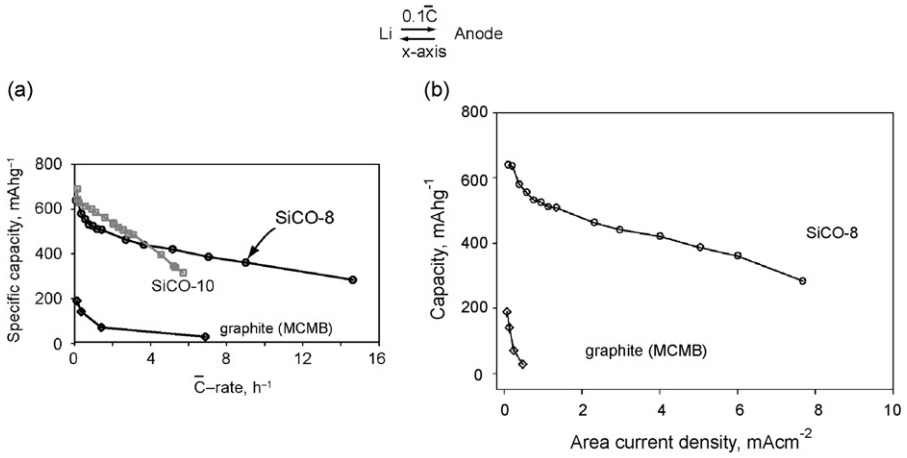

Fig. 7. Capacity loss with C-rate for SiCO specimens, processed at 1000 °C and 800 °C, and in comparison to specimens made from MCMB graphite.

Table 2
Loading density and capacity of MCMB and SiCO-8.

	Loading density (mg cm^{-2})	Delivered capacity at 100 mA g^{-1} (mAh g^{-1})
MCMB	2.35	71
SiCO-8	1.85	637

for extraction was varied as shown by $m\bar{C}$ along the horizontal axis.

A more transparent comparison between SiCO-8 and MCMB is shown in Fig. 7(b), where the capacity is plotted as a function of the current density expressed in units of mA cm^{-2}. The performance of SiCO is far better; furthermore the capacity differential becomes larger at higher current densities. The thickness of the electrode, exemplified by the loading density, that is the weight of the active material per unit area of the anode (mg cm^{-2}) can influence the C-rate performance. A numerical comparison of the capacity for SiCO-8 and MCMB, at comparable loading densities is given in Table 2, showing SiCO possesses a capacity that is nearly an order of magnitude greater than MCMB.

The C-rate experiments were extended up to 40$\bar{C}$ in steps. The insertion rate was held constant at 100 mA g^{-1}, while the extraction rate was increased progressively in steps. At each step the cell was cycled ten times. These results are shown in Fig. 8. Even at the highest rate, a capacity of ~50 mAh g^{-1} is obtained. However, the most significant finding is that the capacity is fully recovered when the C-rate is dropped back to 1/6$\bar{C}$, showing that high rate cycling did not damage the cell.

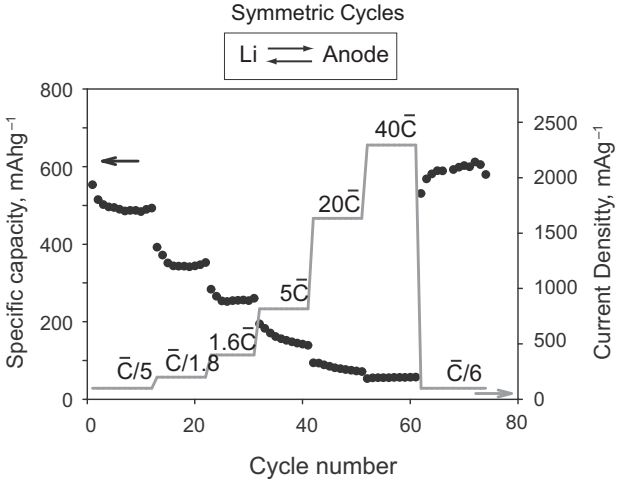

Fig. 8. Very high C-rate performance of SiCO cells without damage (the capacity recovers upon return to low C-rate).

The results in Figs. 7 and 8 suggest fast diffusivity of Li in the PDCs, presumably because of the open and amorphous molecular network structure of the material. The results also confirm the robust nature of this class of materials, which is in accordance with other properties such as high oxidation resistance [12], and resistance to crystallization [9,13] at very high temperatures.

6. Discussion

The results presented in this article have both scientific and technological implications. From the scientific point of view several questions are raised on the relationship between processing, nanostructure and the Li insertion/extraction behavior. For example: why are 800 °C processed sample more stable then samples processed at higher temperature? what is the molecular origin of the ICL and the hysteresis? why does the capacity decrease abruptly as oxygen is replaced by nitrogen?

Some direction to thinking with respect to these queries is provided by phenomenological correlations. It is known that 800 °C processed samples are likely to contain more residual hydrogen than the samples processed at higher temperatures, but less than the specimen processed at 700 °C. NMR studies show that mixed bonds of silicon, carbon and oxygen do not begin to emerge until 800°, and are fully established at ~1000 °C [14]. Therefore it is to be inferred, as has been already shown, that mixed bonds are necessary for high level of Li insertion into PDCs [11]. The question of residual hydrogen at 800 °C imparting greater cyclic stability would appear to be in consonance with the general understanding that Li is more stable when intercalated into carbon structures that contain some hydrogen [15].

The finding that replacing oxygen with nitrogen severely curtails Li capacity is new and scientifically quite interesting. The analysis in Fig. 2 suggests that replacing oxygen with nitrogen renders the mixed bond Si-tetrahedra unable to sequester Li. This is a curious result that can lead to an understanding of how mixed bonds between Si–C–O promote lithium binding with energies of about 0.5 V. It is unlikely that the bonding is ionic (as in Li_2O which would have much greater binding energies). It is more likely that the electronic structure of the mixed bonds can induce a dipole into the Li atom thereby creating a shallow energy well. Mixed bonds that are highly covalent are likely to have highly localized and "stiff"

Table A1
Composition data for the five PDC specimens from current work, and five additional, high nitrogen containing materials selected from Ref. [6].

	Composition (wt.%)				Mole. formula ($SiC_xO_yN_z$)	N/O ratio	Lithium capacity	
	Si	C	O	N			Q_{total} (mAh g^{-1})	Q_{rev} (mAh g^{-1})
PDC-1	62.0	18.6	0.4	19.0	$SiC_{0.70}O_{0.01}N_{0.61}$	61	96	38
PDC-2	52.9	20.6	10.4	16.1	$SiC_{0.91}O_{0.34}N_{0.61}$	1.8	453	237
PDC-3	51.5	23.1	13.0	12.4	$SiC_{1.04}O_{0.44}N_{0.48}$	1.0	912	551
PDC-4	47.8	31.0	16.2	5.0	$SiC_{1.51}O_{0.59}N_{0.21}$	0.4	1094	751
PDC-5	42.8	36.4	20.8	0.0	$SiC_{1.98}O_{0.85}N_{0.00}$	0	1164	794
	55.4	19.9	4.1	20.6	$SiC_{0.84}O_{0.13}N_{0.75}$	5.8	14	6
	54.5	19.9	4.7	20.9	$SiC_{0.85}O_{0.15}N_{0.77}$	5.1	10	7
Ref. [6]	54	16.9	7.2	21.9	$SiC_{0.73}O_{0.23}N_{0.81}$	3.5	44	39
	59.1	17.9	1.3	21.7	$SiC_{0.71}O_{0.04}N_{0.74}$	18.5	27	11
	61.3	20.6	1.7	16.4	$SiC_{0.76}O_{0.05}N_{0.53}$	10.6	15	4

electron densities, which would not be malleable enough to form such induced-dipoles. We note that the electronegativities of O and N are 3.5 and 3.0, respectively. Therefore the Si–N bonds will be more covalent than the Si–O bonds, which favors the argument just presented.

The topic of hysteresis has been considered in depth in Ref. [11], where it was shown that while a part of the hysteresis does arise from the time dependency of insertion and extraction, there is a significant fraction that is intrinsic to the energy barriers to insertion and extraction. An interfacial barrier that favors insertion relative to extraction was proposed as a tentative explanation.

The question of a large ICL in the PDCs remains obscure. In general, one may say that there are "traps" in the structure that serve as a one-way path for Li storage. Perhaps these traps are very small empty volumes in the structure where Li atoms can form clusters, that become essentially metallic and therefore unable to disperse and diffuse out from within the SiCO.

To expand upon the engineering significance of the results presented here, we analyze the performance of full cells based upon the data for the reversible capacity. A balanced full cell, where the anode is assumed to have a capacity of 160 mAh g^{-1}, is considered. The total capacity of the anode–cathode pair is then calculated and the predicted performance of SiCO is compared with graphite [16] and lithium titanate ($Li_4Ti_5O_{12}$) [17].

To calculate the overall gravimetric energy density consider the cathode and the anode to have weights of m_C and m_A, respectively. Their Li capacities are called q_A (for the anode) and q_C for the cathode. A balanced anode–cathode system requires that:

$$q_C m_C = q_A m_A \tag{6}$$

The gravimetric capacity of the balanced anode–cathode pair, m_A, is given by:

$$q* = \frac{q_A m_A}{m_A + m_C} \tag{7}$$

Dividing numerator and denominator in Eq. (5) by m_A, and further substituting from Eq. (4) we obtain the relationship between the total capacity, and the capacities of the electrodes:

$$q* = \frac{q_A}{1 + (q_A/q_C)} \tag{8}$$

Note that $q^* \to q_A$, if $q_C \gg q_A$, and conversely, $q^* \to q_C$ if $q_A \gg q_C$, that is, the total capacity is limited by the electrode having the lower capacity.

The predictions from Eq. (8) are shown in Fig. 9 for the case of $0.1\bar{C}$. Note that the shape of the curve given by Eq. (8) follows a path of diminishing returns as the anode capacity increases above 800 mAh g^{-1}. The current capacity of PDC-anode lies nearly at the top of the rise in total capacity. Therefore, the technological need is not so much to increase the capacity (until cathodes with high capacities become available) but instead to address the issues of ICL and hysteresis, which require a scientific understanding of how these new materials can store large quantities of Li.

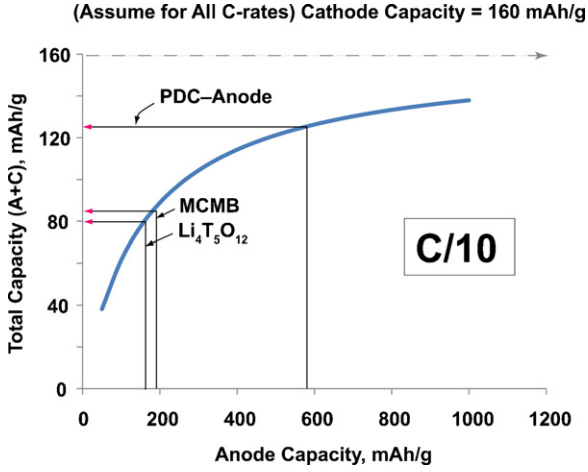

Fig. 9. Gravimetric capacity of full cell assuming a cathode capacity of 160 mAh g^{-1}, and electrode balance.

Acknowledgement

This research was supported by the Ceramics Program of the Division of Material Research at the National Science Foundation under Grant No: 0907108.

Appendix A.

Reports in the literature show that silicon oxycarbides, SiCO [5], have a higher capacity than silicon carbonitrides, SiCN [6].[2] The purpose of the present exercise was to measure the capacity of alloys of SiCO and SiCN, to discover how the capacity varies with the N/O ratio. Note that N and O are equivalent elements in the nanodomain structure sketched in Fig. 1. For example N can be

[2] The accepted protocol for the pyrolysis of PDCs is 1000 °C. Normally, the properties of PDCs are enhanced by the presence of N, therefore, the first step is usually to prepare SiCN samples for the measurement of properties. Thus, the SiCN results presented in the paper were the first to be obtained in our laboratory, and these samples were prepared at 1000 °C. Indeed the exhaustive data for SiCO published in the literature (ref. 5: Wilson et al., 1997) were obtained with samples pyrolyzed at 1000 °C. The results for different processing temperatures were, e.g. 800 °C, were obtained in a subsequent study. The difference between SiCO-800 and SiCO-1000 is indeed subtle: while the SiCO-8 has a highly ICL, it has better stability than SiCO-10. With this in mind, and noting that Li insertion capacity SiCN specimens are very markedly inferior to SiCO, it was not considered to be worthwhile to pursue a comprehensive study of the SiCN materials processed at different temperatures.

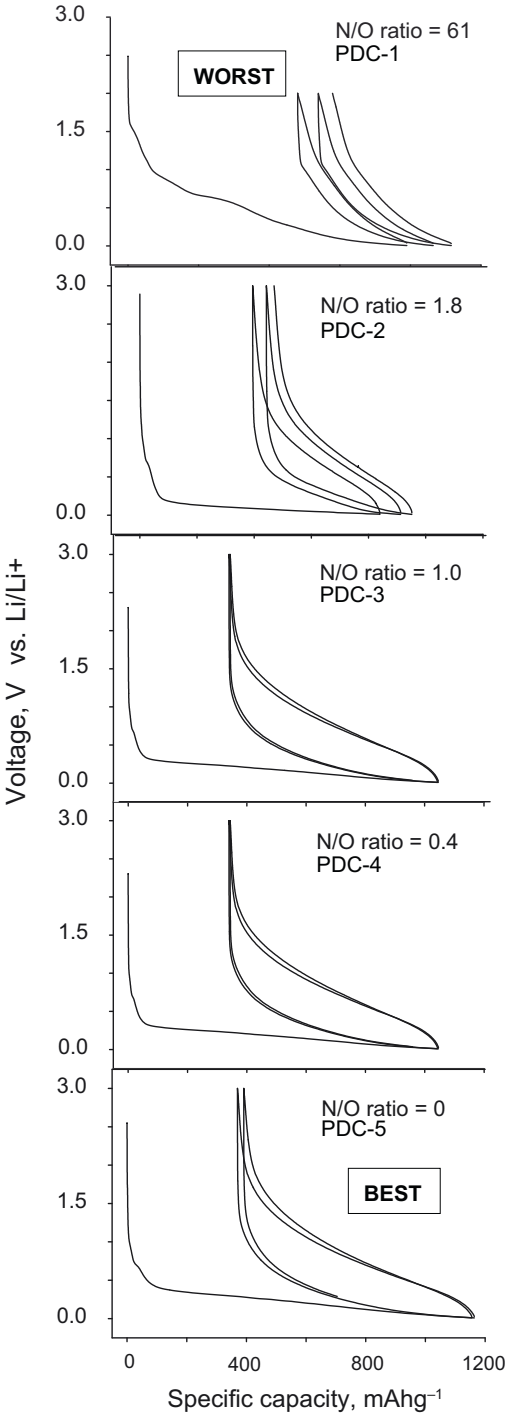

Fig. A1. First three cycles for the five $SiC_xO_yN_z$ specimens. PDC-1 has the lowest and PDC-5 the highest oxygen content.

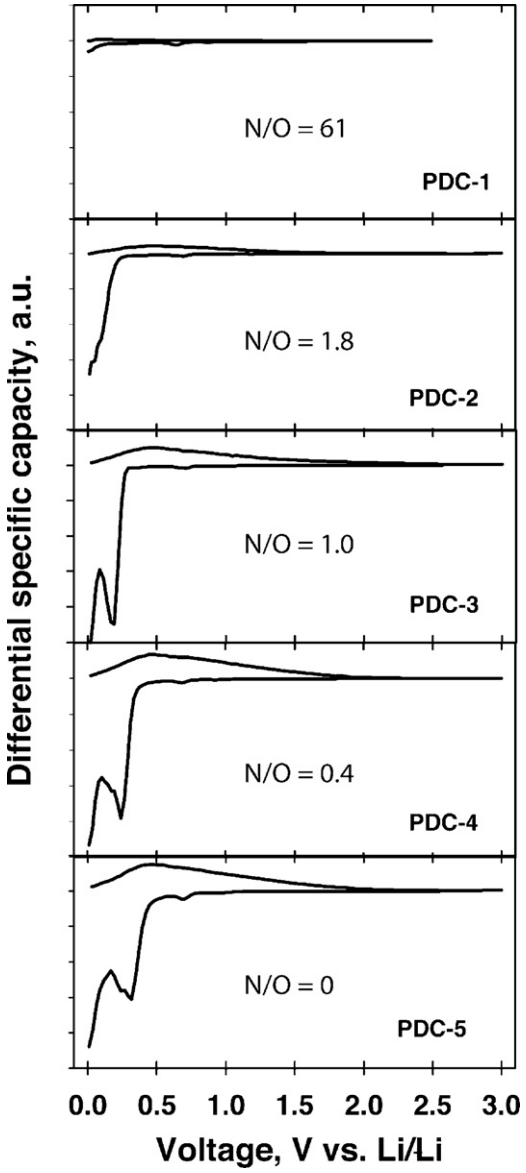

Fig. A2. Differential capacity plots from the data in Fig. A1.

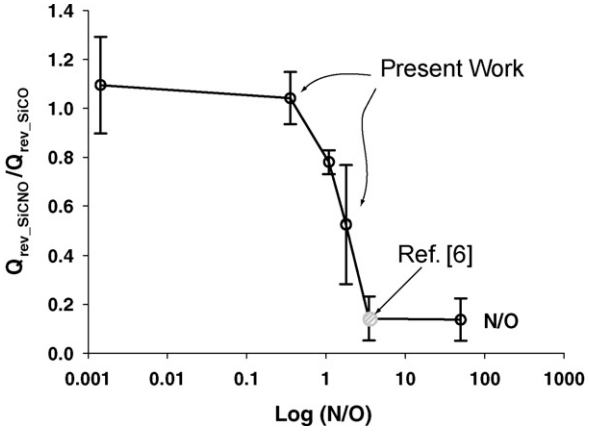

Fig. A3. The normalized capacity of the SiCON materials plotted at a function of the N/O ratio.

substituted for oxygen since both elements bond only to Si in the network: exchanging O by N simply changes the coordination of the Si tetrahedra. However, having a different valency, the nitrogen substitution can significantly influence the electronic structure, and with it, the energetics of Li sequestration. [18]

The compositions of five specimens, PDC-1 thru PDC-5, are shown in Table A1. The weight fractions and the atom concentrations for carbon, oxygen and nitrogen are given. Compositions of five specimens that are predominantly nitrogen containing, listed at the bottom of the figure are extracted from literature [19].

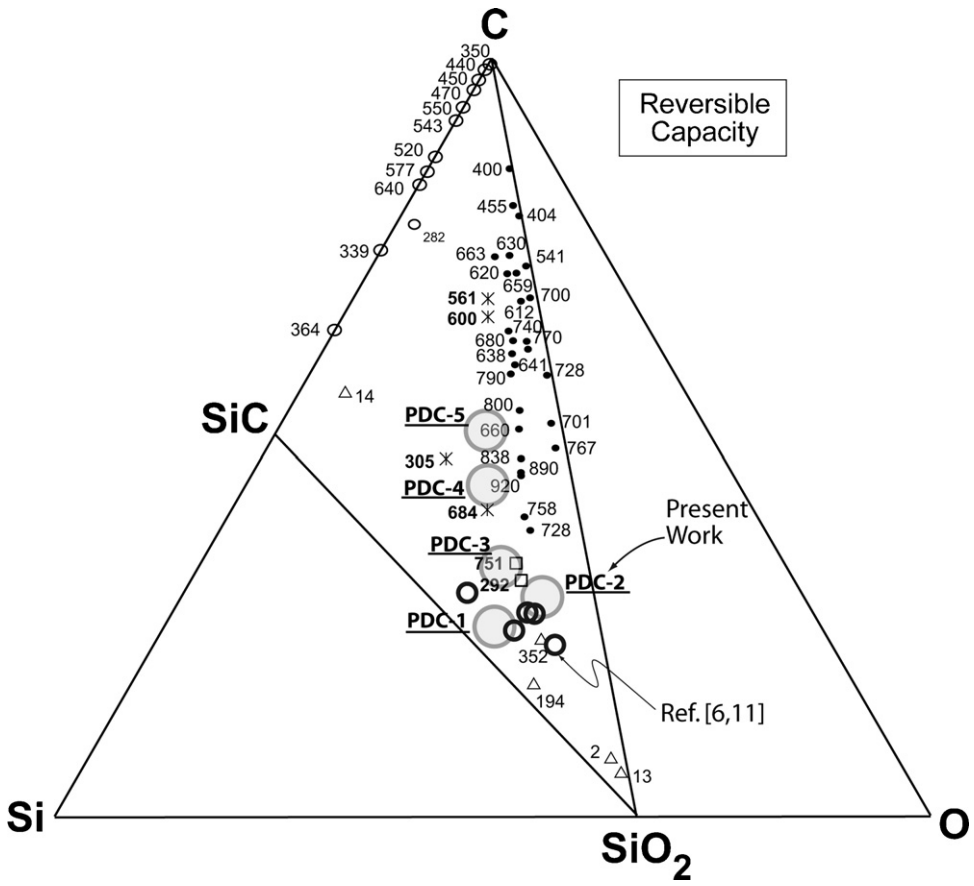

Fig. A4. The SiCO equivalent compositions plotted in the composition diagram which shows the reversible capacites of SiCO specimens over a wide range of compositions from Ref. [6].

The voltage–charge profiles for the first three cycles for PDC-1 to PDC-5 are given in Fig. A1. The total (Q_{total}), and the reversible (Q_{rev}) capacities are included in Table A1. The differential capacity plots (DCP) are given in Fig. A2: they provide information regarding the voltage levels where lithium may react chemically with the PDCs. A peak in the 0.2 V–0.4 V regime is seen for the high oxygen materials, especially PDC-4 and PDC-5. These peaks are absent in the high nitrogen materials like N/O ≈ 61 and 1.8 in Fig. A2.

The data in Table A1 show that the reversible capacity varies significantly with composition (form less than 100 to more than 700 mAh g^{-1}). In general it appears that higher nitrogen content reduces the capacity for lithium. However, in order to obtain a systematic relationship between capacity and N/O molar ratio, it is necessary to account for the variability in the Si and C content (in the case of SiCO materials, it has been shown that these elements also influence the capacity).

To this purpose an "equivalent[3]" SiCO capacity for all specimens listed in Table A1 is estimated using the procedure described in the next paragraph. Then, the measured capacities are normalized against the equivalent SiCO capacity. This ratio of the actual capacity and the equivalent SiCO capacity is plotted against the N/O atom ratio, in Fig. A3. The important result from this figure is that the ratio is relatively insensitive to the nitrogen content as long N/O is less than one but falls sharply when it is greater than one.

[3] The equivalent SiCO capacity for the specimens is obtained in two steps. First the equivalent SiCO composition of SiCNO materials is derived by substituting (4/3)N by (2)O atoms, that is by maintaining the valency balance between oxygen and nitrogen. In the next step the equivalent capacity is estimated by placing the equivalent SiCO composition in the composition diagram, Fig. A4, which shows the measured capacities of SiCO materials over a wide range of SiCO compositions [5,11].

References

[1] U. Kasavajjula, C.S. Wang, A.J. Appleby, Journal of Power Sources (2007) 1631003–1631039.
[2] A. Funabiki, M. Inaba, Z. Ogumi, S. Yuasa, J. Otsuji, A. Tasaka, Journal of the Electrochemical Society 145 (1998) 172–178.
[3] T. Kim, Y.H. Mo, K.S. Nahm, S.M. Oh, Journal of Power Sources 162 (2006) 1275–1281.
[4] M.N. Obrovac, L.J. Krause, Journal of the Electrochemical Society 154 (2007) A103–A108.
[5] A.M. Wilson, G. Zank, K. Eguchi, W. Xing, J.R. Dahn, Journal of Power Sources 68 (1997) 195–200.
[6] R. Kolb, C. Fasel, V. Liebau-Kunzmann, R. Riedel, Journal of the European Ceramic Society 26 (2006) 3903–3908.
[7] A. Saha, R. Raj, D.L. Williamson, Journal of the American Ceramic Society 89 (2006) 2188–2195.
[8] D. Ahn, R. Raj, Journal of Power Sources 195 (2010) 3900–3906.
[9] T. Varga, A. Navrotsky, J.L. Moats, R.M. Morcos, F. Poli, K. Muller, A. Sahay, R. Raj, Journal of the American Ceramic Society 90 (2007) 3213–3219.
[10] G.D. Soraru, L. Pederiva, M. Latournerie, R. Raj, Journal of the American Ceramic Society 85 (2002) 2181–2187.
[11] P.E. Sanchez-Jimenez, R. Raj, Journal of the American Ceramic Society 93 (2010) 1127–1135.
[12] R. Raj, L.N. An, S. Shah, R. Riedel, C. Fasel, H.J. Kleebe, Journal of the American Ceramic Society 84 (2001) 1803–1810.
[13] A. Saha, R. Raj, Journal of the American Ceramic Society 90 (2007) 578–583.
[14] G. Trimmel, R. Badheka, F. Babonneau, J. Latournerie, P. Dempsey, D. Bahloul-Houlier, J. Parmentier, G.D. Soraru, Journal of Sol–Gel Science and Technology 26 (2003) 279–283.
[15] E. Buiel, A.E. George, J.R. Dahn, Journal of the Electrochemical Society 145 (1998) 2252–2257.
[16] Z.X. Shu, R.S. McMillan, J.J. Murray, Journal of the Electrochemical Society 140 (1993) 922–927.
[17] K. Nakahara, R. Nakajima, T. Matsushima, H. Majima, Journal of Power Sources 117 (2003) 131–136.
[18] R. Raj, R. Riedel, G.D. Soraru, Journal of the American Ceramic Society 84 (2001) 2158–2159.
[19] V. Liebau-Kunzmann, C. Fasel, R. Kolb, R. Riedel, Journal of the European Ceramic Society 26 (2006) 3897–3901.